

Magnetism trends in doped Ce-Cu intermetallics in the vicinity of quantum criticality: realistic Kondo lattice models based on dynamical mean-field theory

Munehisa Matsumoto^{1,2}

¹*Institute for Solid State Physics, University of Tokyo, Kashiwa 277-8581, JAPAN*

²*Institute of Materials Structure Science, High Energy Accelerator Research Organization, 1-1 Oho, Tsukuba, Ibaraki 305-0801, Japan*

(Dated: December 20, 2024)

The quantum critical point (QCP) in the archetypical heavy-fermion compound CeCu₆ doped by Au is described, accounting for the localized 4*f*-electron of Ce, using realistic electronic structure calculations combined with dynamical mean-field theory (DMFT). Magnetism trends in Ce(Cu_{1- ϵ} Au _{ϵ})₆ ($0 < \epsilon \ll 1$) are compared with those in Co-doped CeCu₅, which resides on the non-ferromagnetic side of the composition space of one of the earliest rare-earth permanent magnet compounds, Ce(Co,Cu)₅. The construction of a realistic Doniach phase diagram shows that the system crosses over a magnetic quantum critical point in the Kondo lattice in $0.2 < x < 0.4$ of Ce(Cu_{1- x} Co _{x})₅. Comparison between Au-doped CeCu₆ and Co-doped CeCu₅ reveals that the swept region in the vicinity of QCP for the latter thoroughly covers that of the former. The implications of these trends on the coercivity of the bulk rare-earth permanent magnets are discussed.

PACS numbers: 71.27.+a, 75.50.Ww, 75.10.Lp

I. MOTIVATION

While heavy-fermion (HF) materials and rare earth permanent magnets (REPM's) have gone through contemporary developments since the 1960s¹⁻⁹, apparently little overlap has been identified between the two classes of materials. One of the obvious reasons for the absence of mutual interest lies in the difference in the scope of the working temperatures: HF materials typically concern low-temperature physics of the order of 10K or even lower while REPM concerns room temperature at 300K or higher. The other reason is that the interesting regions in the magnetic phase diagram sit on the opposite sides, where HF behavior appears around a region where magnetism disappears⁶ while with REPM the obvious interest lies in the middle of a ferromagnetic phase. In retrospect, several common threads in the developments for HF compounds and REPM's can be seen: one of the earliest REPM's was Ce(Co,Cu)₅⁴ where Cu was added to CeCo₅ to implement coercivity, and CeCu₅ was eventually to be identified as an antiferromagnetic Kondo lattice^{10,11}.

One of the representative HF compounds is CeCu₆^{12,13} that was discovered almost at the same time as the champion magnet compound Nd₂Fe₁₄B^{8,9,14}. While REPM's make a significant part in the most important materials in the upcoming decades for a sustainable solution of the energy problem with their utility in traction motors of (hybrid) electric vehicles and power generators, HF materials might remain to be mostly of academic interests. But we note that a good permanent magnet is made of a ferromagnetic main-phase and less ferromagnetic sub-phases. For the latter compounds in REPM's, we discuss possible common physics with HF materials, namely, magnetic quantum criticality where magnetism disappears and associated scales in space-time fluctuations diverge, and propose one of the possible solutions

for a practical problem on how to implement coercivity, which measures robustness of the metastable state with magnetization against externally applied magnetic fields.

Even though the mechanism of bulk coercivity on the macroscopic scale in REPM's is not entirely understood, the overall multiple-scale structure has been clear in that the intrinsic properties of materials on the microscopic scale of the scale of $O(1)$ nm is carried over to the macroscopic scale via mesoscopic scale. Namely, possible scenarios in coercivity of Nd-Fe-B magnets^{15,16} and Sm-Co magnets¹⁷ have been so far discussed as follows.

a. Nd-Fe-B magnets Propagating domain walls around a nucleation center of reversed magnetization are blocked before going too far. Infiltrated elemental Nd in the grain-boundary region that is paramagnetic in the typical operation temperature range of $O(100)$ K neutralizes inter-granular magnetic couplings among Nd₂Fe₁₄B grains¹⁸. Single-phase Nd₂Fe₁₄B does not show coercivity at room temperature and fabrication of an optimal microstructure on the mesoscopic scale, with the infiltrated Nd metals between Nd₂Fe₁₄B grains, seems to be crucial to observe bulk coercivity.

b. Sm-Co magnets and Ce analogues Pinning centers of domain walls are distributed over cell-boundary phases made of Sm(Co,Cu)₅ which separate hexagonally-shaped cells of Sm₂(Co,Fe)₁₇. The uniformity of the cell boundary phase^{17,19} suggests that the pinning intrinsically happens on the microscopic scale in Sm(Co,Cu)₅ which freezes out the magnetization reversal dynamics. Also for CeCo₅, addition of Cu has been found to help the development of bulk coercivity⁴ without much particular feature in the microstructure, suggesting here again an intrinsic origin contributing to the bulk coercivity.

Solution of the overall coercivity problem takes out-of-equilibrium statistical physics, multi-scale simulations involving the morphology of the microstructure in the intermetallic materials, electronic correlation in 4*f*-

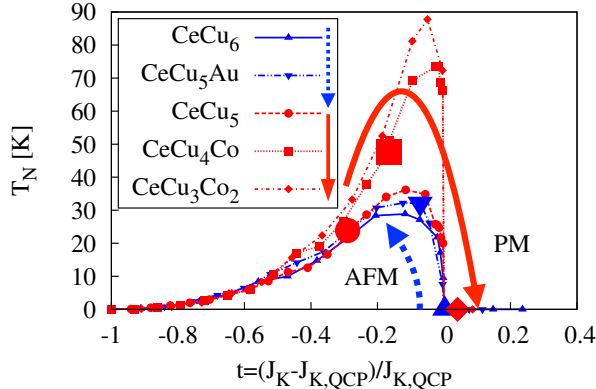


FIG. 1. (Color online) Realistic Doniach phase diagram for the target compounds with a rescaled horizontal axis to measure an effective distance to the magnetic quantum critical point for each target compound. There are the antiferromagnetic (AFM) phase and the Kondo-screened paramagnetic (PM) phase. It is seen that Co-doped CeCu_5 moves from the magnetic side towards the Kondo-screened phase crossing QCP, while Au-doped CeCu_6 moves to the opposite direction. Arrows are guide for the eye.

electrons, finite-temperature magnetism of Fe-based ferromagnets, and magnetic anisotropy, each of which by itself makes a subfield for intensive studies. Faced with such a seemingly intractable problem, it is important to build up fundamental understanding step by step. Therefore, we clarify the magnetism trends around quantum criticality in Ce-Cu intermetallics, as a part of $4f$ - $3d$ intermetallics that belong to a common thread between HF materials and REPM, in order to pin-point a possible intrinsic contribution to the coercivity, specifically via exponentially growing length scales in spatial correlation and characteristic time in the dynamics.

The magnetization in REPM's derives from $3d$ -electron ferromagnetism coming from Fe-group elements and $4f$ -electrons in rare-earth elements provide the uni-axial magnetic anisotropy for the intrinsic origin of coercivity. Sub-phases are preferably free from ferromagnetism to help coercivity e.g. by stopping the propagation of domain walls. In the practical fabrication of REPM, both of the main-phase compound and other compounds for sub-phases should come out of a pool of the given set of ingredient elements. Investigations on non-ferromagnetic materials that appear in the same composition space as the ferromagnetic material are of crucial importance for contributing the intrinsic information into the solution of the coercivity problem.

Thus we investigate the Cu-rich side of the composition space in $\text{Ce}(\text{Co},\text{Cu})_5$ and inspect the magnetism trends around the HF compound, CeCu_5 . It is found that Co doping into CeCu_5 drives the material toward a magnetic quantum critical point (QCP), to the extent that

$3d$ -electron ferromagnetism coming from Co does not dominate, which seems to be the case experimentally²⁰ when the concentration of Co is below 40%. It has also been known that Au-doped CeCu_6 goes into quantum criticality^{21,22}, a trend which is reproduced in the same simulation framework. With CeCu_6 as one of the most representative HF materials, experimental measurements and theoretical developments²³⁻²⁵ have been extensively done. Our finding basically reproduces what has already been agreed on the location of magnetic QCP, but the spirit of our microscopic description may not entirely be the same as some of the past theoretical works²³⁻²⁵. Our description should be more consistent with even older works²⁶ in the fundamental spirit with the proper incorporation of realistic energy scales based on electronic structure calculations. We may fail in catching some subtlety specific to Au-doped CeCu_6 , but our approach should be suited rather for general purposes in providing an overview over intrinsic magnetism of f - d intermetallics to extract the common physics therein.

We set up a realistic Kondo lattice model^{27,28} for these cases and see the followings: 1) CeCu_6 sits very close to the QCP, 2) Au-induced QCP can also be described on the basis of a conventional Kondo lattice model as down-folded from realistic electronic structure data featuring localized $4f$ -electrons, at least concerning the relative location of QCP, without invoking valence fluctuations²⁹ or the specialized Kondo-Heisenberg model to describe local quantum criticality²³⁻²⁵, in contrast to some of those previous developments^{23,24,29} for Au-doped CeCu_6 , and 3) Co-doping in CeCu_5 drives the material toward the QCP in the opposite direction as Au-doping does in CeCu_6 . The main results are summarized in Fig. 1 where the Au-doped CeCu_6 and Co-doped CeCu_5 are located around a magnetic QCP following a rescaled realistic Doniach phase diagram^{6,27,28}.

The rest of the paper is organized as follows. In the next section we describe our methods^{27,28} as specifically applied to the target materials: pristine CeCu_6 , CeCu_5 , and doped cases. In Sec. III magnetism trends in the target materials are clarified. In Sec. IV several issues remaining in the present descriptions and possible implications from HF physics on the intrinsic part of the solution of the coercivity problem of REPM are discussed. The final section is devoted to the conclusions and outlook.

II. METHODS AND TARGET MATERIALS

We combine *ab initio* electronic structure calculations on the basis of the full-potential linear muffin-tin orbital method^{30,31} and dynamical mean-field theory (DMFT) for a Kondo lattice model with well-localized $4f$ -electrons³²⁻³⁴, to construct a Doniach phase diagram⁶ adapted for a given target material to identify an effective distance of the material to a magnetic quantum critical point. Electronic structure calculations follow density

functional theory (DFT)^{35,36} within the local density approximation (LDA)^{36,37}. Our realistic simulation framework can be regarded as a simplified approach inspired by LDA+DMFT^{38,39}, where electronic structure calculations describing the relatively high-energy scales and a solution of the embedded impurity problem in the lowest energy scales are bridged: here a realistic Kondo lattice model is downfolded⁴⁰ from the electronic structure calculations for Ce-based compounds with well localized $4f$ -electrons^{27,28}.

More specifically, our computational framework is made of the following two steps:

1. For a given target material, LDA+Hubbard-I^{39,41} is done to extract hybridization between localized $4f$ -electrons and conduction electrons, $-\Im\Delta(\omega)/\pi$ as a function of energy $\hbar\omega$ around the Fermi level. Position of the local $4f$ -electron level below the Fermi level is determined as well.
2. A realistic Kondo lattice model (KLM) with the Kondo coupling J_K is defined following the relations²⁷:

$$J_K = |V|^2 \left[\frac{1}{|\epsilon_f|} + \frac{1}{(\epsilon_f + U_{ff} - J_{\text{Hund}})} \right], \quad (1)$$

$$|V|^2 \equiv -\frac{1}{\pi} \int_{-\infty}^D d\omega \frac{\text{Tr}\Im\Delta(\omega)}{N_F}, \quad (2)$$

which is a realistic adaptation of Schrieffer-Wolff transformation⁴² to map the Anderson model²⁶ to Kondo model. Here U_{ff} and J_{Hund} are the Coulomb repulsion energy and an effective Hund coupling between $4f$ electrons, respectively, in $(4f)^2$ configuration and D is an energy cutoff^{27,40} that defines the working energy window for the realistic Schrieffer-Wolff transformation. The trace in Eq. (2) is taken over all $4f$ -orbitals and dividing the traced hybridization by $N_F \equiv 14$ gives the strength of hybridization per each orbital. Experimental information on the local level splittings is incorporated for the $4f$ -electron part. The thus defined KLM is solved within DMFT using the continuous-time Monte Carlo impurity solver³². A Doniach phase diagram⁶ separating the magnetic phase and paramagnetic phase is constructed for each of the target materials and the magnetic QCP is located.

The realistic model parameters that appear in Eqs. (1) and (2) are taken on an empirical basis referring to past works^{39,43}, among which the origin of the on-site Coulomb repulsion energy $U_{ff} = 5$ eV between $4f$ -electrons can be traced partly back to past electronic structure calculations⁴⁴ and analyses of photoemission spectroscopy data⁴⁵. Even though one can argue for material-specific data of U_{ff} , here we are more concerned with relative trends among the target materials within a realistic model with fixed parameters

compound	a (a.u.), $b/a, c/a$
CeCu ₆	$a = 15.3295, b/a = 0.62894, c/a = 1.25271$ Ref. 46
CeCu ₅ Au	$a = 15.5902, b/a = 0.61624, c/a = 1.25576$ Ref. 47
CeCu ₅	$a = 9.702, b/a = 1, c/a = 0.79957$ Ref. 20
CeCu ₄ Co	(fixed to be the same as CeCu ₅)
CeCu ₃ Co ₂	(fixed to be the same as CeCu ₅)

TABLE I. Inputs to LDA+Hubbard-I: the lattice constants of each target compound.

to get an overview over a group of Ce-based compounds with well localized $4f$ -electrons, rather than pursuing preciseness of each material-specific data point.

Below we describe the details of the overall procedure one by one, taking CeCu₆ as a representative case, partly introducing the results.

A. LDA+Hubbard-I

The overall initial input here is the experimental lattice structure. This is taken from the past experimental literature for pristine CeCu₆ in Ref. 46 and CeCu₅ in Ref. 20, and also for CeCu₅Au in Ref. 47 together with the particular site preference of the dopant atom, Au. Our input lattice constants are summarized in Table I. We note that CeCu₆ undergoes a structural phase transition between a high-temperature orthorhombic phase⁴⁶ and a low-temperature monoclinic phase⁴⁸, while CeCu₅Au does not⁴⁹. In order to compare CeCu₆ and CeCu₅Au on an equal footing and inspect the relative trends between them and observing that the lattice distortion introduced by the structure transition seems to be minor⁴⁹, we fix the working lattice structure of CeCu₆ to be the orthorhombic phase and proceed to the downfolding to the realistic Kondo-lattice model. The internal coordinates of atoms in CeCu₆ and CeCu₅Au are shown in Table II. For Co-doped CeCu₅, various things happen in real experiments starting with the introduction of a ferromagnetic conduction band coming from Co and lattice shrinkage even before reaching the valence transition on the Co-rich side. Here in order to simplify the problem and to focus on the magnetism trends concerning the $4f$ -electron QCP, we fix the working lattice to be that of pristine CeCu₅ and inspect the effects of replacements of Cu by Co. Following the site preference of Co for Cu($3g$) site as suggested in Ref. 50 for Cu-substituted YCo₅, which we also confirm in separate calculations⁵¹, we replace Cu by Co in the $3g$ sublattice one by one as shown in Table. III for CeCu₄Co and CeCu₃Co₂. With this particular set-up, the effects of Co-doping on CeCu₅ has been effectively softened in our calculations. However we will see that Co-doping on CeCu₅ drives the material across the QCP more effectively than Au-doping does for CeCu₆.

LDA+Hubbard-I calculations give the hybridization

(a)		
atom	Wyckoff	internal coordinate
Ce	4c	(0.2602, 0.2500, 0.4354)
Cu(1)	8d	(0.4354, 0.0041, 0.1908)
Cu(2)	4c	(0.1467, 0.2500, 0.1418)
Cu(3)	4c	(0.1821, 0.7500, 0.2451)
Cu(4)	4c	(0.4380, 0.7500, 0.4023)
Cu(5)	4c	(0.0987, 0.7500, 0.4846)

(b)		
atom	Wyckoff	internal coordinate
Ce	4c	(0.26078, 0.2500, 0.43593)
Cu(1)	8d	(0.43493, 0.0013, 0.18791)
Au	4c	(0.14216, 0.2500, 0.13897)
Cu(3)	4c	(0.18475, 0.7500, 0.25071)
Cu(4)	4c	(0.44400, 0.7500, 0.39553)
Cu(5)	4c	(0.09178, 0.7500, 0.48395)

TABLE II. Inputs to LDA+Hubbard-I: internal coordinates of atoms in the orthorhombic (Space Group No.62) unit cell of (a) CeCu₆ and (b) CeCu₅Au. The spatial translation vectors are plainly (1, 0, 0), (0, 1, 0), and (0, 0, 1), measured with respect to the lattice constants as the unit length. Each atom in the unit cell has been specified with the Wyckoff position and the internal coordinate. The input data are taken from (a) Ref. 46 and (b) Ref. 47. It is to be noted that all of the atoms contribute 4 atoms except for Cu(1) that contributes to 8 atoms to the unit cell made of 4 formula units. Au has been selectively put into the Cu(2) site⁴⁷.

atom	Wyckoff	internal coordinate
Ce	1a	(0, 0, 0)
Cu	2c	(1/2, 1/(2√3), 0)
Cu	2c	(1/2, -1/(2√3), 0)
Cu	3g	(1/4, -√3/4, 1/2)
(Cu/Co) ^a	3g	(1/4, √3/4, 1/2)
(Cu/Co) ^b	3g	(1/2, 0, 1/2)

^aCu for CeCu₅ and CeCu₄Co / Co for CeCu₃Co₂

^bCu for CeCu₅ / Co for CeCu₄Co and CeCu₃Co₂

TABLE III. Inputs to LDA+Hubbard-I: internal coordinates of the atoms in the hexagonal (Space Group No. 191) unit cell of CeCu₅, CeCu₄Co, and CeCu₃Co₂. Here the spatial translation vectors are taken as (-1/2, √3/2, 0), (1/2, √3/2, 0), and (0, 0, 1). In contrast to Table II, all of the constituent atoms in the same sublattice specified with the Wyckoff position are explicitly shown since the replacement of atoms happens for a selection of the atoms in the Cu(3g) sublattice.

$-\Im\Delta(\omega)/\pi$ and position of the local 4*f*-level, ϵ_f . The results for ϵ_f and $|V|^2$ as defined in Eq. (2) are summarized in Table IV. Raw data for $-\Im\Delta(\omega)/\pi$ as traced over all of the 4*f*-orbitals is shown in Fig. 2.

compound	ϵ_f (eV)	$ V ^2$
CeCu ₆	-1.61	0.172967
CeCu ₅ Au	-1.81	0.159501
CeCu ₅	-2.02	0.157148
CeCu ₄ Co	-1.99	0.156348
CeCu ₃ Co ₂	-1.72	0.157907

TABLE IV. Outputs of LDA+Hubbard-I: calculated position of localized 4*f*-electron level, ϵ_f , where the offset is taken at the Fermi level, is shown in the second column for each target compound. In the third column, the integrated hybridization as defined in Eq. (2) is shown.

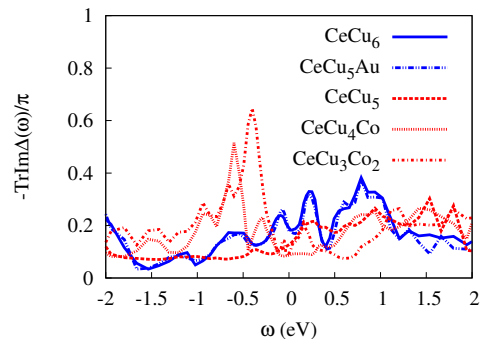


FIG. 2. (Color online) Calculated hybridization function for the target compounds within LDA+Hubbard-I.

B. DMFT for the realistic Kondo lattice model

Following Ref. 27, the hybridization function between the localized 4*f*-orbital in Ce and conduction electron band defines the material-specific KLM. Here we describe the details of the Kondo impurity problem embedded in the KLM within DMFT⁵² where we use the continuous-time quantum Monte Carlo solver⁵³ for the Kondo impurity problem³².

In the impurity problem embedded in DMFT we incorporate the realistic crystal-field and spin-orbit level splittings in the local 4*f*-orbital of Ce. The local 4*f*-

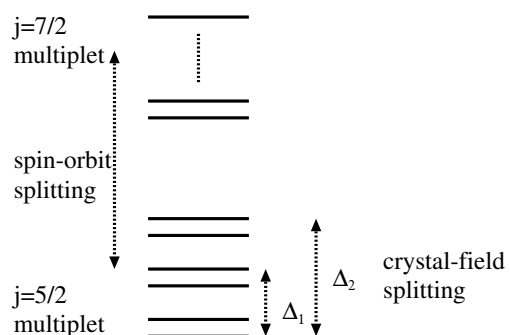


FIG. 3. Schematic picture for local-level splitting caused by spin-orbit interaction and crystal fields.

compound	crystal-field splittings
CeCu ₆	$\Delta_1 = 7$ meV, $\Delta_2 = 13$ meV Ref. 54
CeCu ₅	$\Delta_1 \simeq \Delta_2 = 17$ meV Ref. 55

TABLE V. Input crystal-field splittings following past neutron scattering experiments.

electron level scheme is shown in Fig. 3. For CeCu₆ and hexagonal CeCu₅, it is known that the crystal structure splits the $j = 5/2$ multiplets into three doublets, separated by Δ_1 (meV) between the lowest doublet and the second-lowest doublet, and Δ_2 (meV) between the lowest doublet and the third-lowest doublet. Crystal-field splittings have been taken from the past neutron scattering experiments as summarized in Table V. We set the level splitting between $j = 5/2$ and $j = 7/2$ multiplets due to spin-orbit interaction to be $\Delta_{\text{spin-orbit}} = 0.3$ (eV) referring to the standard situation in Ce-based HF compounds⁵⁶.

The input obtained with LDA+Hubbard-I to our Kondo problem is shown in Fig. 2. The Kondo coupling J_K via a realistic variant²⁷ of the Schrieffer-Wolff transformation⁴² is defined as in Eqs. (1) and (2). There D was the band cutoff that is set to be equal to the Coulomb repulsion $U_{ff} = 5$ (eV), and J_{Hund} is the effective Hund coupling in the f^2 multiplet to which the second term of Eq. (1) describes the virtual excitation from the $(4f)^1$ ground state.

We sweep J_{Hund} to locate the QCP on a Doniach phase diagram and also to pick up the realistic data point at $J_{\text{Hund}} = 1$ (eV). This particular choice of the Hund coupling in the virtually excited state $(4f)^2$ has been motivated^{43,57} by the typical intra-shell direct exchange coupling of $O(1)$ eV and an overall magnetism trend in CeM₂Si₂ (M=Au, Ag, Pd, Rh, Cu, and Ru), CeTIn₅ (T=Co, Rh, and Ir) and pressure-induced quantum critical point in CeRhIn₅ as studied in our previous works, Ref. 27, 28, and 58, respectively. Thus the working computational setup has been applied to elucidate the magnetism trends around QCP as precisely as have been done for other representative HF compounds. In practice, we define J_K at $J_{\text{Hund}} = 0$ as $J_{K,0}$ and then sweep a multiplicative factor $\alpha = J_K/J_{K,0}$, calculating the temperature dependence of staggered magnetic susceptibility $\chi(\pi, T)$ for each α . In this way we can see where in the neighborhood of the QCP our target material with α corresponding to the realistic number, $J_{\text{Hund}} = 1$ eV, resides on the Doniach phase diagram.

We calculate the staggered magnetic susceptibility $\chi(\pi)$ with the two-particle Green's function following the formalism developed in Ref. 34 and using a random-dispersion approximation to decouple it into single-particle Green's functions⁵⁹ which would enhance the transition temperature, in addition to the single-site mean-field nature in DMFT. The calculated data for $1/\chi(\pi)$ is shown in Fig. 4 for the case of CeCu₆. The temperature dependence of the reciprocal of the stag-

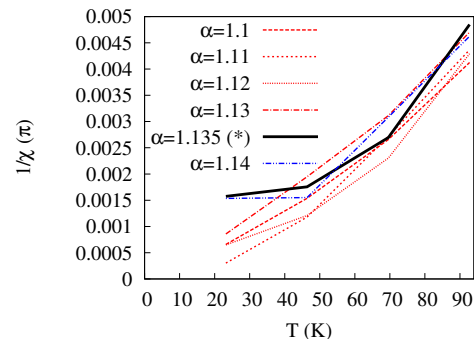


FIG. 4. (Color online) Calculated temperature dependence of the reciprocal of staggered magnetic susceptibility for CeCu₆, the reference compound. The data with $\alpha = 1.135$, specified with an asterisk, corresponds to the realistic data point.

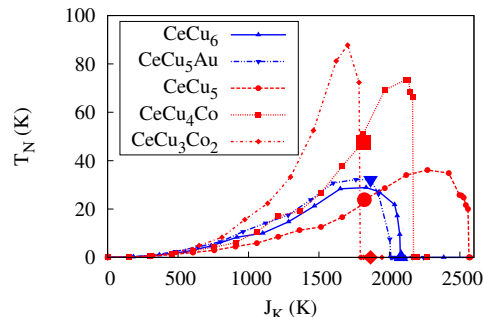


FIG. 5. (Color online) Realistic Doniach phase diagram for the target compounds with the bare energy scale of the Kondo couplings.

gered magnetic susceptibility $1/\chi(\pi)$ is observed for each $J_K = \alpha J_{K,0}$ and we extrapolate it linearly to the low temperature region to see if there is a finite Néel temperature. We identify that the Néel temperature vanishes in the parameter range $1.13J_{K,0} < J_K < 1.135J_{K,0}$, where $J_{K,0}$ is the Kondo coupling at $J_{\text{Hund}} = 0$. The realistic data point is obtained by plugging in $J_{\text{Hund}} = 1$ (eV)²⁷ and $\epsilon_f = -1.61$ (eV) (as can be found in Table IV) to Eq. (1) to be $J_K = 1.1347J_{K,0}$. Thus the data in Fig. 4 shows that CeCu₆ is almost right on the magnetic QCP where the Néel temperature disappears.

The same procedures are applied to all other target materials.

III. RESULTS

Plotting calculated Néel temperatures with respect to $J_K = \alpha J_{K,0}$, the Doniach phase diagram is constructed for each target material as shown in Fig. 5.

By rescaling the horizontal axis of the Doniach phase diagram as follows, $t \equiv (J_K - J_{K,\text{QCP}})/J_{K,\text{QCP}}$ to inspect

the dimensionless distance to the QCP independently of the materials^{27,28}, we end up with the main results as shown in Fig. 1.

A. CeCu₆ vs CeCu₅

Remarkably, CeCu₆ falls almost right on top of magnetic QCP in Fig. 5. Also it is seen that the energy scales for antiferromagnetic order are on the same scale for CeCu₆ and CeCu₅ as seen in the vertical-axis scales for the calculated Néel temperatures. This may be reasonable considering the similar chemical composition between CeCu₆ and CeCu₅.

Here we note that overestimates of the calculated Néel temperature are unavoidable due to the single-site nature of DMFT and approximations involved in the estimation of two-particle Green's function²⁷. Thus the calculated Néel temperature for CeCu₅ falling in the range of 20K should be compared to the experimental value of 4K^{10,11} only semi-quantitatively. Nevertheless, expecting that the same degree of systematic deviations are present in all of the data for the target compounds, we can safely inspect the relative trends between CeCu₆ and CeCu₅.

B. Magnetic QCP in Au-doped CeCu₆

In Fig. 5 it is seen that doping Au into CeCu₆ only slightly shifts the energy scales competing between magnetic ordering and Kondo screening. Most importantly, Au-doping drives the material towards the antiferromagnetic phase and the magnetic QCP is identified in the region Ce(Cu_{1- ϵ} Au ϵ)₆ with $\epsilon \ll 1$, which is consistent with the experimental trends of magnetism^{21,22}. This has been achieved with the control of an effective degeneracy of orbitals incorporating the realistic width of level splittings in the localized 4*f*-orbital, putting the characteristic energy scales in magnetism under good numerical control in the present modeling.

While quantitative success for Ce(Cu_{1- ϵ} Au ϵ)₆ ($0 \leq \epsilon \ll 1$) concerning the location of the magnetic QCP is seen, some qualitative issues may be considered to be on the way to address magnetic quantum criticality, since this particular materials family represents the local quantum criticality scenario²³⁻²⁵ where a sudden breakdown of the Kondo effect is discussed to occur on the basis of a Kondo-Heisenberg model. In our realistic model, the exchange interaction between localized 4*f*-electrons naturally come in as a second-order perturbation process with respect to the Kondo coupling⁶⁰, which is the RKKY interaction⁶⁰⁻⁶².

Even though no special place for another Heisenberg term is identified in our realistic Kondo lattice model, there should indeed be other terms that are not explicitly considered: for example, with very well localized 4*f*-electrons, there is another indirect exchange coupling⁶³ that work via the following two-steps: (a) intra-atomic

exchange coupling between 4*f*-spin and 5*d*-spin and (b) inter-atomic hybridization between 5*d*-band and other conduction band. Notably, in this channel the coupling between 5*d* and 4*f* is ferromagnetic, which is in principle in competition against the antiferromagnetic Kondo coupling that we mainly consider here.

For REPM compounds such as Nd-Fe intermetallics, the latter indirect exchange coupling, which we denote J_{RT} for the convenience of reference as the effective coupling between rare-earth elements and transition metals, is dominant because 4*f*-electrons are even more well localized than in Ce³⁺-based compounds. There the Kondo couplings are not in operation practically, since *f-c* hybridization is weak and Kondo couplings are at too small energy scales as compared to other exchange couplings. Now that we bring HF materials and REPM compounds on the same playground, the *f-d* indirect exchange couplings should also have been given more attention even though there is at the moment only some restricted prescriptions^{64,65} to downfold a realistic number into J_{RT} .

This indirect exchange coupling can motivate the Heisenberg term on top of the realistic Kondo lattice model, even though it is to be noted that the sign of such extra Heisenberg terms is ferromagnetic. This may pave the way to define a realistic version of the Kondo-Heisenberg model²³⁻²⁵. Since J_{RT} 's can compete against RKKY at most only on the same order, the presence of the J_{RT} terms would not significantly alter the position of magnetic QCP, which is brought about by the Kondo coupling that competes against RKKY as a function of exponential of the reciprocal of the coupling constants. This way, it is hoped that there might be a way to reconcile the local QCP scenario for Au-doped CeCu₆ and the present realistic modeling for the magnetic QCP focusing on the characteristic energy scales involving the Kondo effect.

Recent time-resolved measurements and theoretical analyses based on DMFT^{67,68} for Ce(Cu,Au)₆ also provides a way to reconcile the local QCP scenario and experimentally detected signals from the possible Kondo quasiparticles on the real-time axis within the non-crossing approximation (NCA)^{69,70} as the impurity solver in DMFT. Since our DMFT results are based on quantum Monte Carlo (QMC) formulated on the imaginary-time axis, migrating to the real-time data via analytic continuation poses a challenging problem^{71,72}, while the solution of the quantum many-body problem is numerically exact with QMC. Thus the location of QCP derived from static observables would be better addressed with the present framework.

Still our numerically exact solution is limited to the imaginary-time direction and effects of the real-space fluctuations are not incorporated in the single-site DMFT. Recently, theoretical comparison between an exact solution of the lattice problem and DMFT has been done⁷³ and an artifact of DMFT to overestimate the region of antiferromagnetic phase has been demonstrated. In this respect, the present location of magnetic QCP

right below CeCu_6 should also reflect the same artifact: if the spatial fluctuations are properly accounted for, the magnetic phase would shrink and the position of CeCu_6 would shift slightly toward the paramagnetic side.

C. QCP to which CeCu_5 is driven by Co-doping

Co-doping in CeCu_5 shifts the energy scales more strongly than seen in Au-doped CeCu_6 . It is seen in Fig. 5 that the QCP is driven toward the smaller J_K side, reflecting the underlying physics that Kondo-screening energy scale is enhanced as Co replaces Cu. The origin of the enhanced Kondo screening is seen in Fig. 2 where anomalous peaks below the Fermi level are coming in which should come from the almost ferromagnetic conduction band which grows into the ferromagnetism in the Co-rich side of the composition space in $\text{Ce}(\text{Cu},\text{Co})_5$. With 40% of Co, the $4f$ -electron QCP is already passed and CeCu_3Co_2 resides in the Kondo-screened phase. Thus it is found that the magnetic QCP of $\text{Ce}(\text{Cu}_{1-x}\text{Co}_x)_5$ is located in $0.2 < x_c < 0.4$. We note that the crystal structure and crystal-field splitting have been fixed to be that of the host material CeCu_5 . In reality, the QCP may be encountered with smaller Co concentration.

In the present simulations, we have neglected the possible ferromagnetism in the ground state contributed by the $3d$ -electrons in Co. Referring to the past experiments for $\text{Ce}(\text{Cu},\text{Co})_5$ described in Ref. 20, the absence of the observed Curie temperatures for the Cu-rich side with the concentration of Cu beyond 60% in the low-temperature region seems to be consistent with our computational setup in the present simulations. Even though other past work⁷⁴ for an analogous materials family $\text{Sm}(\text{Co},\text{Cu})_5$ does show residual Curie temperature in the Cu-rich region, it should be noted that there is a qualitative difference in the nature of the conduction band of Cu-rich materials for the Sm and Ce-based families.

D. Universal and contrasting trends

Co-doped CeCu_5 and Au-doped CeCu_6 represent the different mechanisms where Co enhances f - d hybridization with the $3d$ -electron magnetic fluctuations in the conduction electrons, while Au rather weakens f - d hybridization, being without d -electron magnetic fluctuations.

The trend in magnetism comes from the relative strength of exchange coupling between localized $4f$ -electron and delocalized conduction electrons. Among Ce-based intermetallic compounds, a general trend in the hybridization Δ is seen to be like the following

$$J_K(\text{Ce-Au}) < J_K(\text{Ce-Cu}) < J_K(\text{Ce-Co}) \quad (3)$$

as is partly seen in Ref. 75 for other materials family CeT_2Si_2 (T =transition metals) - somewhere in the se-

quence of the trend written schematically in Eq. (3), a magnetic quantum critical point between antiferromagnetism located on the relatively left-hand side and paramagnetism located on the relatively right-hand side is encountered within the range where $3d$ -electron ferromagnetism from Co does not dominate. The overall one-way trend from antiferromagnetism on the left-most-hand side to paramagnetism on the right-most-hand side in Eq. (3) is universal around the magnetic quantum criticality, while the contrasting trend between Au-doped case and Co-doped case in Ce-Cu intermetallics is seen from the position of the Ce-Cu intermetallics concerning the directions toward which the dopant elements drive.

The opposing trends coming from $3d$ -metal dopant and $5d$ -metal dopant might help in implementing a fine-tuning of the material in a desired proximity to QCP in a possible materials design for REPM's as discussed below in Sec. IV B.

IV. DISCUSSIONS

A. Validity range of the Kondo lattice model

While we have defined the Kondo lattice model referring to the electronic structure of the target materials, the limitations on the validity range of such downfolding approach^{27,40} should be kept in mind in assessing the implications of the present results. In Sec. III B, we have already discussed the possible relation of our model to the Kondo-Heisenberg model that has been extensively used in the local QCP scenario²³⁻²⁵ for $\text{Ce}(\text{Cu}_{1-\epsilon}\text{Au}_\epsilon)_6$. In a wider context, the spirit of the so-called s - d exchange model that was originally introduced by Vonsovskii⁷⁶ and Zener⁷⁷ in the early days of the theory of ferromagnetism is still alive in the indirect exchange coupling J_{RT} . This has been dropped in the present modeling for Ce-based compounds. Here we have assumed that the localization of the $4f$ -electron in our Ce^{3+} -based compounds is good enough to assure the applicability of the Kondo lattice model: at the same time, it is presumed that our $4f$ -electrons in Ce^{3+} -based f - d intermetallics are not so well localized as are the case in Pr^{3+} or Nd^{3+} -based f - d intermetallics. This means that the Kondo coupling coming from f - c hybridization would dominate over the J_{RT} 's coming from the indirect exchange coupling⁶³. Such subtle interplay between different exchange mechanisms can depend on the material. Since we did not address J_{RT} in the present studies, the outcome of the possibly competing exchange interactions is not included in the present scope. Possible subtle aspects coming from the local QCP scenario might reside in this particular leftover region. If one would further opt for an alternative scenario⁷⁸, it may be useful to further investigate the effect of these dropped terms, and include them through improved algorithms based on better intuition. Although a completely *ab initio* description is desirable, to make the problem tractable we are forced into making some

approximations. Here it is at least postulated that the validity of the relative location of magnetic QCP can be assured in the present description because we have put the most sensitive coupling channel, Kondo physics, under good numerical control.

A few more discussions on the validity range of the Kondo lattice model and possible extensions are in order:

1. *Toward more unbiased downfolding*

The terms in our low-energy effective models have been defined targeting at the particular physics, namely, the RKKY interaction and Kondo physics. While this strategy has been good enough to address the relative trends among the target materials around the magnetic QCP, it may well have happened that other relevant terms have been dropped that do not significantly affect the location of QCP. In this regard it may be preferred either a) to downfold from the realistic electronic structure to the low-energy effective models in a more unbiased way, at least proposing all possible candidate terms and eliminating some of them only in the final stage according to a transparent criterion e.g. referring to the relevant energy window or b) to work on the observables directly from first principles without downfolding. While b) does not look very feasible, a) might pose a feasibly challenging problem with a possible help from machine learning⁷⁹ in systematically classifying the candidate terms even for such materials with multiple sublattices, multiple orbitals and relatively large number of orbital degeneracy as imposed from d -electrons and f -electrons.

2. *Effects of valence fluctuations*

Valence fluctuations have not been entirely incorporated in the present description of Ce compounds. Other scenario for Au-doped CeCu₆ that emphasizes the relevance of valence fluctuations are recently discussed²⁹. We have described at least the magnetism trends around the QCP in CeCu₆ and CeCu₅Au only with localized $4f$ -electrons. Apparently valence fluctuations may not be dominant at least for magnetism. We can restore the charge degrees of freedom for $4f$ -electrons and run an analogous set of simulations for a realistic Anderson lattice model in order to see any qualitative difference comes up on top of the localized $4f$ -electron physics. Often the typical valence states for Ce, Ce⁴⁺ or Ce³⁺, are not so clearly distinguished: even in the present Kondo lattice description, $(4f)^0$ state with Ce⁴⁺ are virtually involved in the Kondo coupling and localized $4f$ -electrons even contribute to the Fermi surface⁸⁰. To pick up a few more cases, for actinides or α -Ce, one can either discuss on the basis of localized f -electrons and define the Kondo screening energy scale spanning up to 1000K, or convincing arguments can be done also on the basis of delocalized $4f$ -electrons emphasizing the major roles played by

valence fluctuations. Given that it does not seem quite clear how precisely the relevance or irrelevance of valence fluctuations should be formulated for the description of magnetism trends, here we would claim only the relative simplicity of our description for magnetic QCP in Ce(Cu_{1- ϵ} Au _{ϵ})₆ ($\epsilon \ll 1$). This simplification may well come with the restricted validity range.

B. **Implications on the coercivity of REPM**

Observing that the magnetic QCP can be encountered in the chemical composition space of Ce(Cu,Co)₅, we note that slowing down of spin dynamics when the system crosses over to QCP can be exploited in intrinsically blocking the magnetization reversal processes in REPM to help the coercivity. Since coercivity is a macroscopic and off-equilibrium notion, it is still much under development to formulate a theoretical bridge over the gap between the microscopic equilibrium properties and macroscopic coercivity. At least with QCP, diverging length scales of fluctuations and diverging relaxation times can in principle reach the macroscopically relevant spatial and time scales to help coercivity. Range of the critical region on the temperature axis and on the composition space would depend on each specific case.

In Sm-Co magnets, even though it is clear that the cell boundary phase intrinsically carries the coercivity^{3,17,19}, precise characterization of the inter-relation among the intrinsic properties, microstructure, and coercivity has been still under investigation^{17,19,81}. Since Sm(Cu,Co)₅ can be considered as a hole analogue of Ce(Cu,Co)₅ in the lowest $j = 5/2$ multiplet of Ce³⁺, with a quest for QCP both for magnetism and possibly also for valence fluctuations, it may help to consider the possible role of QCP in Sm(Cu,Co)₅ for the intrinsic part of the coercivity mechanism. Considering the electron-hole analogy, possible effect from QCP for Sm(Cu_{1- x'} Co _{x'})₅ can be expected in the concentration range $x'_c \simeq 1 - x_c$ (here x_c is defined in Sec. III C) which fall in $0.8 > x'_c > 0.6$. This may be compared favorably with the experimentally discussed³ concentration of Cu in Sm-Co magnets, where up to around 35% of Cu in the cell-boundary phase made of Sm(Co,Cu)₅, especially in the triple-junction area^{82,83}, has been correlated with the emergence of good coercivity.

V. **CONCLUSIONS AND OUTLOOK**

Realistic modeling for Au-doped CeCu₆ and Co-doped CeCu₅ successfully describes the trends in magnetism involving QCP on the basis of the localized $4f$ -electrons. One of the archetypical HF materials family, CeCu₆, and its Au-doping-induced QCP can be described within a magnetic mechanism with the terms that can be naturally downfolded from the realistic electronic structure in the spirit of the Anderson model²⁶, without explicitly

invoking valence fluctuations or introducing additional Heisenberg terms. We believe we have just put the characteristic energy scales of the target materials around QCP under good numerical control in having succeeded in addressing the relative trends in magnetism around QCP. We do not rule out other subtlety around QCP that may come from other terms^{23–25} that are not included in the present simulation framework. As long as the dominating energy scales are concerned, those other terms would not significantly alter the magnetism trend around QCP.

Co-doping in CeCu₅ drives the material on a wider scale on the chemical composition axis as compared to Au-doped CeCu₆. This is caused by magnetic fluctuations in the paramagnetic conduction band that is on the verge of ferromagnetism. For the $4f$ - $3d$ intermetallic paramagnets in REPM in general, small changes in the $3d$ -metal concentration can drive the material around in the proximity of quantum criticality on the chemical composition space, rendering it easy to encounter critical regions in a microstructure with an appropriate spatial variance in the microchemistry.

Ce(Co,Cu)₅ represents one of the earliest and most typical materials family in REPM^{14,84}. The lattice structure of the materials family RT₅ including Ce(Co,Cu)₅ can be transformed into R₂T₁₇ and RT₁₂⁸⁴ (R=rare earth and T=Fe group elements), and a local structure around the rare-earth sites in the champion magnet com-

pound R₂Fe₁₄B (R=rare earth) resembles RT₅ as described in Sec. III A of Ref. 14. With our results for Ce(Cu,Co)₅ in relation to Ce(Cu,Au)₆ concerning QCP, it has been suggested that potentially various properties of derived compounds from the RT₅ archetypical series⁸⁵ residing in REPM, especially physics in the crossover to QCP, can be exploited for the possible intrinsic contribution to coercivity.

ACKNOWLEDGMENTS

MM's work in ISSP, University of Tokyo is supported by Toyota Motor Corporation. The author thanks C. E. Patrick for his careful reading of the manuscript. The author benefited from comments given by J. Otsuki and H. Sepehri-Amin. The author gratefully acknowledges helpful discussions with H. Shishido, T. Ueno, K. Saito in related projects, crucial suggestions given by T. Akiya pointing to the particular materials family R(Cu,Co)₅ (R=rare earth), and an informative lecture given by K. Hono in the early stage of this project. The present work was partly supported by JSPS KAKENHI Grant No. 15K13525. Numerical computations were executed on ISSP Supercomputer Center, University of Tokyo and Numerical Materials Simulator in National Institute for Materials Science.

-
- ¹ J. Kondo, Resistance Minimum in Dilute Magnetic Alloys, *Prog. Theor. Phys.* **32**, 37 (1964).
 - ² G. Hoffer and K. J. Strnat, Magnetocrystalline Anisotropy of YCo₅ and Y₂Co₁₇, *IEEE Trans. Mag.* **MAG-2**, 487 (1966).
 - ³ E. A. Nesbitt, R. H. Willens, R. C. Sherwood, E. Buehler, and J. H. Wernick, New Permanent Magnet Materials, *Appl. Phys. Lett.* **12**, 361 (1968).
 - ⁴ Y. Tawara and H. Senno, Cerium, Cobalt, and Copper Alloy as a Permanent Magnet Material, *Japan. J. Appl. Phys.* **7**, 966 (1968).
 - ⁵ K. Andres, J. E. Graebner, and H. R. Ott, $4f$ -Virtual-Bound-State Formation in CeAl₃ at Low Temperatures, *Phys. Rev. Lett.* **35**, 1779 (1975).
 - ⁶ S. Doniach, The Kondo lattice and Weak Antiferromagnetism, *Physica* **91B**, 231 (1977).
 - ⁷ F. Steglich, J. Aarts, C. D. Bredl, W. Lieke, D. Meschede, W. Franz, and H. Schäfer, Superconductivity in the Presence of Strong Pauli Paramagnetism: CeCu₂Si₂ *Phys. Rev. Lett.* **43**, 1892 (1979).
 - ⁸ M. Sagawa, S. Fujimura, N. Togawa, H. Yamamoto, and Y. Matsuura, New material for permanent magnets on a base of Nd and Fe, *J. Appl. Phys.* **55**, 2083 (1984).
 - ⁹ J. J. Croat, J. F. Herbst, R. W. Lee, and F. E. Pinkerton, Pr-Fe and Nd-Fe-based materials: A new class of high-performance permanent magnets, *J. Appl. Phys.* **55**, 2078 (1984).
 - ¹⁰ E. Bauer, E. Gratz, and C. Schmitzer, CeCu₅: Another Kondo Lattice Showing Magnetic Order, *J. Magn. Magn. Mater.* **63 & 64**, 37 (1987).
 - ¹¹ For a review, see E. Bauer, Anomalous properties of Ce-Cu- and Yb-Cu-based compounds, *Adv. Phys.* **40**, 417 (1991).
 - ¹² Y. Onuki, Y. Shimizu, T. Komatsubara, Magnetic Property of a New Kondo Lattice Intermetallic Compound: CeCu₆, *J. Phys. Soc. Jpn.* **53**, 1210 (1984).
 - ¹³ G. R. Stewart, Z. Fisk, and M. S. Wire, New Ce heavy-fermion system: CeCu₆, *Phys. Rev. B* **30**, 482 (1984).
 - ¹⁴ For a review, see J. F. Herbst, R₂Fe₁₄B materials: Intrinsic properties and technological aspects, *Rev. Mod. Phys.* **63**, 819 (1991).
 - ¹⁵ K. Hono and H. Sepehri-Amin, Strategy for high-coercivity Nd-Fe-B magnets, *Scr. Mater.* **67**, 530 (2012).
 - ¹⁶ K. Hono and H. Sepehri-Amin, Prospect for HRE-free high coercivity Nd-Fe-B permanent magnets, *Scr. Mater.* **151**, 6 (2018).
 - ¹⁷ For a review, see K. Ohashi, Present and Future of Sm₂Co₁₇ Magnets, *J. Japan Inst. Metals* **76**, 96 (2012) (in Japanese except for abstract, key words, and figure captions).
 - ¹⁸ Y. Murakami, T. Tanigaki, T. T. Sasaki, Y. Takeno, H. S. Park, T. Matsuda, T. Ohkubo, K. Hono, D. Shindo, Magnetism of ultrathin intergranular boundary regions in Nd-Fe-B permanent magnets, *Acta Mater.* **71** 370 (2014).
 - ¹⁹ H. Sepehri-Amin, J. Thielsch, J. Fischbacher, T. Ohkubo, T. Schrefl, O. Gutfleisch, K. Hono, Correlation of microchemistry of cell boundary phase and interface structure to the coercivity of Sm(Co_{0.784}Fe_{0.100}Cu_{0.088}Zr_{0.028})_{7.19} sin-

- tered magnets, *Act. Mater.* **126**, 1 (2017).
- ²⁰ D. Girodin, C. H. Allibert, F. Givord, and R. Lemaire, Phase Equilibria in the CeCo₅-CeCu₅ System and Structural Characterization of the Ce(Co_{1-x}Cu_x)₅ Phases, *J. Less Common Metals* **110**, 149 (1985).
- ²¹ H. v. Löhneysen, T. Pietrus, G. Portisch, H. G. Schlager, A. Schröder, M. Sieck, T. Trappmann, Non-Fermi-liquid behavior in a heavy-fermion alloy at a magnetic instability, *Phys. Rev. Lett.* **72**, 3262 (1994).
- ²² A. Schröder, G. Aeppli, R. Coldea, M. Adams, O. Stockert, H. v. Löhneysen, E. Bucher, R. Ramazashvili, P. Coleman, Onset of antiferromagnetism in heavy-fermion metals, *Nature* **407**, 351 (2000).
- ²³ Q. Si, S. Rabello, K. Ingersent, J. L. Smith, Locally critical quantum phase transitions in strongly correlated metals, *Nature* **413**, 804 (2001).
- ²⁴ P. Coleman, C. Pépin, Q. Si, and R. Ramazashvili, How do Fermi liquids get heavy and die, *J. Phys. Condens. Matter* **13**, R723 (2001).
- ²⁵ For a recent review, see e.g. S. Kirchner, S. Paschen, Q. Chen, S. Wirth, D. Feng, J. D. Thompson, and Q. Si, Colloquium: Heavy-electron quantum criticality and single-particle spectroscopy, *Rev. Mod. Phys.* **92**, 011002 (2020).
- ²⁶ P. W. Anderson, Localized Magnetic States in Metals, *Phys. Rev.* **124**, 41 (1961).
- ²⁷ M. Matsumoto, M.-J. Han, J. Otsuki, S. Y. Savrasov, First-Principles Simulations of Heavy Fermion Cerium Compounds Based on the Kondo Lattice, *Phys. Rev. Lett.* **103**, 096403 (2009).
- ²⁸ M. Matsumoto, M.-J. Han, J. Otsuki, S. Y. Savrasov, Magnetic quantum critical point and dimensionality trend in cerium-based heavy-fermion compounds, *Phys. Rev. B* **82**, 180515(R) (2010).
- ²⁹ G. W. Scheerer, Z. Ren, S. Watanabe, G. Lapertot, D. Aoki, D. Jaccard, K. Miyake, The dominant role of critical valence fluctuations on high T_c superconductivity in heavy fermions, *npj Quantum Materials* **3**, 41 (2018).
- ³⁰ O. K. Andersen, Linear methods in band theory, *Phys. Rev. B* **12**, 3060 (1975).
- ³¹ For the material-specific calculation of the hybridization function, we use linear muffin-tin orbital method using the code described in S. Y. Savrasov, Linear-response theory and lattice dynamics: A muffin-tin-orbital approach, *Phys. Rev. B* **54**, 16470 (1996).
- ³² J. Otsuki, H. Kusunose, P. Werner and Y. Kuramoto, Continuous-Time Quantum Monte Carlo Method for the Coqblin-Schrieffer Model, *J. Phys. Soc. Jpn.* **76**, 114707 (2007).
- ³³ J. Otsuki, H. Kusunose, and Y. Kuramoto, The Kondo Lattice Model in Infinite Dimensions: I. Formalism, *J. Phys. Soc. Jpn.* **78**, 014702 (2009).
- ³⁴ J. Otsuki, H. Kusunose, and Y. Kuramoto, The Kondo Lattice Model in Infinite Dimensions: II. Static Susceptibilities and Phase Diagram, *J. Phys. Soc. Jpn.* **78**, 034719 (2009).
- ³⁵ P. Hohenberg and W. Kohn, Inhomogeneous Electron Gas, *Phys. Rev.* **136**, B864 (1964).
- ³⁶ W. Kohn and L. J. Sham, Self-Consistent Equations Including Exchange and Correlation Effects, *Phys. Rev.* **140**, A1133 (1965).
- ³⁷ S. H. Vosko, L. Wilk, and M. Nusair, Accurate spin-dependent electron liquid correlation energies for local spin density calculations: a critical analysis, *Can. J. Phys.* **58**, 1200 (1980).
- ³⁸ For a review up to late 1990's, see V. I. Anisimov, A. I. Poteryaev, M. A. Korotin, A. O. Anokhin, and G. Kotliar, First-principles calculations of the electronic structure and spectra of strongly correlated systems: dynamical mean-field theory, *J. Phys.: Condens. Matter* **9** 7359 (1997).
- ³⁹ For a review up to mid 2000's, see G. Kotliar, S. Y. Savrasov, K. Haule, V. S. Oudovenko, O. Parcollet, C. A. Marianetti, Electronic structure calculations with dynamical mean-field theory, *Rev. Mod. Phys.* **78**, 865 (2006).
- ⁴⁰ for a review including the fundamental aspects of down-folding to low-energy effective models from electronic structure calculations and the relative nature of the effective models defined with respect to the working energy window as introduced by the energy cutoff, see M. Imada and T. Miyake, *J. Phys. Soc. Jpn.* **79**, 112001 (2010).
- ⁴¹ J. Hubbard, *Proc. R. Soc. Lond. A* **276**, 238 (1963); *ibid* **277**, 237 (1964); *ibid* **281**, 401 (1964).
- ⁴² J. R. Schrieffer and P. A. Wolff, Relation between the Anderson and Kondo Hamiltonians, *Phys. Rev.* **149**, 491 (1966).
- ⁴³ R. D. Cowan, *The Theory of Atomic Structure and Spectra* (University of California Press, Berkeley, Los Angeles, London, 1981).
- ⁴⁴ J. F. Herbst, R. E. Watson, J. W. Wilkins, Relativistic calculations of 4*f* excitation energies in the rare-earth metals: Further results, *Phys. Rev. B* **17**, 3089 (1978), and references therein.
- ⁴⁵ Y. Baer and J. K. Lang, High-energy spectroscopy of f^{n+1} and f^{n-1} states in rare-earth metals, *J. Appl. Phys.* **50**, 7485 (1979).
- ⁴⁶ D. T. Cromer, A. C. Larson, R. B. Roof Jr., The Crystal Structure of CeCu₆, *Acta Cryst.* **13**, 913 (1960).
- ⁴⁷ M. Ruck, G. Portisch, H. G. Schlager, M. Sieck, H. v. Löhneysen, Structure and electrical resistivity of the heavy fermion compound CeCu₅Au, *Acta Cryst. B* **49**, 936 (1993).
- ⁴⁸ H. Asano, M. Umino, Y. Ōnuki, T. Komatsubara, F. Izumi, N. Watanabe, Neutron diffraction study on the low-temperature monoclinic form of CeCu₆, *J. Phys. Soc. Jpn.* **55**, 454 (1986).
- ⁴⁹ K. Grube, W. H. Fietz, U. Tutsch, O. Stockert and H. v. Löhneysen, Suppression of the structural phase transition in CeCu₆ by pressure and Au doping, *Phys. Rev. B* **60**, 11947 (1999).
- ⁵⁰ K. Uebayashi, K. Terao, H. Hamada, First principle calculation for preferential site occupation of 3d transition-metal atoms in YCo₅ and YNi₅, *J. Alloys Compd.* **346**, 47 (2002).
- ⁵¹ M. Matsumoto, in preparation.
- ⁵² A. Georges, G. Kotliar, W. Krauth, M. J. Rozenberg, Dynamical mean-field theory of strongly correlated fermion systems and the limit of infinite dimensions, *Rev. Mod. Phys.* **68**, 13 (1996).
- ⁵³ P. Werner, A. Comanac, L. de' Medici, M. Troyer, and A. J. Millis, Continuous-Time Solver for Quantum Impurity Models, *Phys. Rev. Lett.* **97**, 076405 (2006); P. Werner and A. J. Millis, Hybridization expansion impurity solver: General formulation and application to Kondo lattice and two-orbital models, *Phys. Rev. B* **74**, 155107 (2006).
- ⁵⁴ U. Witte, R. Schedler, O. Stockert, and M. Loewen-

- haupt, The Investigation of the Crystalline Electric Field of CeCu_2 and CeCu_6 , *J. Low Temp. Phys.*, **147**, 97 (2007).
- ⁵⁵ D. Gignoux, D. Schmitt, E. Bauer, A. P. Murani, Inelastic Neutron Scattering in Some hexagonal Cerium Compounds, *J. Magn. Magn. Matter* **88**, 63 (1990).
- ⁵⁶ for a review, see R. Settai, T. Takeuchi, Y. Onuki, Recent Advances in Ce-Based Heavy-Fermion Superconductivity and Fermi Surface Properties, *J. Phys. Soc. Jpn.* **76**, 051003 (2007).
- ⁵⁷ B. Mühlischlegel, Relation between the Anderson and Kondo Hamiltonians for the case of degenerate impurity orbitals, *Z. Phys.* **208**, 94 (1968).
- ⁵⁸ M. Matsumoto, Navigating the Trends in the Proximity to Magnetic Quantum Critical Point and Superconductivity for Ce-Based Heavy-Fermion Compounds, *J. Phys. Soc. Jpn.* **88**, 114705 (2019).
- ⁵⁹ F. Gebhard, *The Mott Metal-Insulator Transition*, Springer Tracts in Modern Physics Vol. 137 (Springer-Verlag, Berlin, 1997).
- ⁶⁰ K. Yosida, Magnetic Properties of Cu-Mn Alloys, *Phys. Rev.* **106**, 893 (1957).
- ⁶¹ M. A. Ruderman and C. Kittel, Indirect Exchange Coupling of Nuclear Magnetic Moments by Conduction Electrons, *Phys. Rev.* **96**, 99 (1954).
- ⁶² T. Kasuya, A Theory of Metallic Ferro- and Antiferromagnetism on Zener's Model, *Prog. Theor. Phys.* **16**, 45 (1956).
- ⁶³ I. A. Campbell, Indirect exchange for rare earths in metals, *J. Phys. F: Met. Phys.* **2**, L47 (1972).
- ⁶⁴ In our related work: M. Matsumoto, H. Akai, Y. Harashima, S. Doi, T. Miyake, Relevance of $4f$ - $3d$ exchange to finite-temperature magnetism of rare-earth permanent magnets: An *ab-initio*-based spin model approach for NdFe_{12}N , *J. Appl. Phys.* **119**, 213901 (2016) a manual rescaling of J_{RT} was attempted on top of a set of *ab initio* numbers for $3d$ - $5d$ exchange couplings that are calculated following Ref. 66.
- ⁶⁵ Y. Toga, M. Matsumoto, S. Miyashita, H. Akai, S. Doi, T. Miyake, A. Sakuma, Monte Carlo analysis for finite-temperature magnetism of $\text{Nd}_2\text{Fe}_{14}\text{B}$ permanent magnet, *Phys. Rev. B* **94**, 174433 (2016).
- ⁶⁶ A. I. Liechtenstein, A. I. Liechtenstein, M. I. Katsnelson, V. P. Antropov, and V. A. Gubanov, Local spin density functional approach to the theory of exchange interactions in ferromagnetic metals and alloys, *J. Magn. Magn. Mater.* **67**, 65 (1987).
- ⁶⁷ C. Wetli, S. Pal, J. Kroha, K. Kliemt, C. Krellner, O. Stockert, H. v. Löhneysen, and M. Fiebig, Time-resolved collapse and revival of the Kondo state near a quantum phase transition, *Nat. Phys.* **14**, 1103 (2018).
- ⁶⁸ S. Pal, C. Wetli, F. Zamani, O. Stockert, H. v. Löhneysen, M. Fiebig, and J. Kroha, Fermi Volume Evolution and Crystal-Field Excitations in Heavy-Fermion Compounds Probed by Time-Domain Terahertz Spectroscopy, *Phys. Rev. Lett.* **122**, 096401 (2019).
- ⁶⁹ Y. Kuramoto, Self-consistent perturbation theory for dynamics of valence fluctuations I. Single-site theory, *Z. Phys. B* **53**, 37 (1983).
- ⁷⁰ For a review, see e.g. N. E. Bickers, Review of techniques in the large-N expansion for dilute magnetic alloys, *Rev. Mod. Phys.* **59**, 845 (1987).
- ⁷¹ For a review, see e.g. M. Jarrel and J. E. Gubernatis, *Phys. Rep.* **269**, 133 (1996).
- ⁷² For recent developments, see e.g. J. Otsuki, M. Ohzeki, H. Shinaoka, K. Yoshimi, Sparse modeling approach to analytical continuation of imaginary-time quantum Monte Carlo data, *Phys. Rev. E* **95**, 061302(R) (2017); H. Shinaoka, J. Otsuki, M. Ohzeki, K. Yoshimi, Compressing Green's function using intermediate representation between imaginary-time and real-frequency domains, *Phys. Rev. B* **96**, 035147 (2017).
- ⁷³ T. Schäfer, A. A. Katanin, M. Kitatani, A. Toschi, and K. Held, Quantum Criticality in the Two-Dimensional Periodic Anderson Model, *Phys. Rev. Lett.* **122**, 227201 (2019).
- ⁷⁴ E. Lectard, C. H. Allibert, R. Ballou, Saturation magnetization and anisotropy fields in the $\text{Sm}(\text{Co}_{1-x}\text{Cu}_x)_5$ phases, *J. Appl. Phys.* **75**, 6277 (1994).
- ⁷⁵ T. Endstra, G. J. Nieuwenhuys, and J. A. Mydosh, Hybridization model for the magnetic-ordering behavior of uranium- and cerium-based 1:2:2 intermetallic compounds, *Phys. Rev. B* **48**, 9595 (1993).
- ⁷⁶ S. V. Vonsovskii, *Zh. Eksp. Teor. Fiz.* **16**, 981 (1946) [*Sov. Phys. JETP* **10**, 468 (1946)].
- ⁷⁷ C. Zener, Interaction between the d Shells in the Transition Metals, *Phys. Rev.* **81**, 440 (1951).
- ⁷⁸ N. E. Sluchanko, On the limits of application of Anderson and Kondo models in physics of strongly correlated electron systems, *Low Temperature Physics* **41**, 699 (2015), and references therein.
- ⁷⁹ For a review on recent developments, see e.g. G. Carleo, I. Cirac, K. Cranmer, L. Daudet, M. Schuld, N. Tishby, L. Vogt-Maranto, and L. Zdeborová, Machine learning and the physical sciences, *Rev. Mod. Phys.* **91**, 045002 (2019).
- ⁸⁰ J. Otsuki, H. Kusunose, Y. Kuramoto, Evolution of a Large Fermi Surface in the Kondo Lattice, *Phys. Rev. Lett.* **102**, 017202 (2009).
- ⁸¹ C. E. Patrick, M. Matsumoto, J. B. Staunton, First-principles calculations of the magnetocrystalline anisotropy of the prototype 2:17 cell boundary phase $\text{Y}(\text{Co}_{1-x-y}\text{Fe}_x\text{Cu}_y)_5$, *J. Magn. Magn. Mater.* **477**, 147 (2019).
- ⁸² Y. Zhang, W. Tang, G. C. Hadjipanayis, C. Chen, C. Nelson, and K. Krishnan, *IEEE Trans. Magn.* **37**, 2525 (2001).
- ⁸³ X. Y. Xiong, T. Ohkubo, T. Koyama, K. Ohashi, Y. Tawara, K. Hono, The microstructure of sintered $\text{Sm}(\text{Co}_{0.72}\text{Fe}_{0.20}\text{Cu}_{0.055}\text{Zr}_{0.025})_{7.5}$ permanent magnet studied by atom probe, *Acta Mater.* **52**, 737 (2004).
- ⁸⁴ H. S. Li and J. M. D. Coey, Magnetic Properties of Ternary Rare-Earth Transition-metal Compounds, *Handbook of Magnetic Materials*, **6**, Ch. 1 (Edited by K. H. J. Buschow).
- ⁸⁵ For a recent thorough investigation from first principles over the series RCO_5 , see e.g. C. E. Patrick and J. B. Staunton, Temperature-dependent magnetocrystalline anisotropy of rare earth/transition metal permanent magnets from first principles: The light RCO_5 ($R=\text{Y}$, La-Gd) intermetallics, *Phys. Rev. Materials* **3**, 101401(R) (2019).